Journal of Physics:
Condensed Matter

PAPER • **OPEN ACCESS**

A triad of high-field magnetic transitions in V_5S_8

To cite this article: C A Sonego *et al* 2026 *J. Phys.: Condens. Matter* **38** 025801

IOP Publishing J. Phys.: Condens. Matter 38 (2026) 025801 https://doi.org/10.1088/1361-648X/ae2b41

Journal of Physics: Condensed Matter

OPEN ACCESS

RECEIVED
28 August 2025

REVISED
17 November 2025

ACCEPTED FOR PUBLICATION
10 December 2025

PUBLISHED
9 January 2026

PAPER

A triad of high-field magnetic transitions in V_5S_8

C A Sonego[1,2], P M T Vianez[1], H Li[1], J C Lashley[1], G G Lonzarich[1], M N Ali[3], M A Avila[2] and S E Rowley[1,*]

[1] Cavendish Laboratory, University of Cambridge, J. J. Thomson Avenue, Cambridge CB3 0HE, United Kingdom
[2] CCNH, Universidade Federal do ABC, Santo André, São Paulo, Brazil
[3] Kavli Institute of Nanoscience, Delft University of Technology, Delft, The Netherlands
[*] Author to whom any correspondence should be addressed.

E-mail: ser41@cam.ac.uk

Keywords: magnetism, vanadium sulphide, high-field spin transitions, magnetoresistance, V&lt, sub&gt, 5&lt, /sub&gt, S&lt, sub&gt, 8&lt, /sub&gt, quantum phase transitions, magnetic transitions

Abstract

We report the observation of an unexpected phase transition at high magnetic fields between the spin-flop and spin-flip transitions in the d-electron antiferromagnetic metal V_5S_8. High-precision magnetic, thermal and electrical transport measurements enable the transitions to be tracked up to fields as high as 35 T and at temperatures down to the milli-kelvin range revealing three distinct magnetic quantum phase transitions. We present a model that finds agreement with our observation of a triad of spin transitions involving two sublattices with frustrated inter-and intra-sublattice spin couplings.

1. Introduction

The chalcogenides V_xS_8, in which x can vary between 4 and 8, form an interesting family of narrow-band d-electron metals that host a wide range of charge and magnetic order at low temperatures upon variations of stoichiometry and pressure. VS_2 ($x = 4$) is a charge-density-wave metal below approximately 300 K [1, 2], V_5S_8 ($x = 5$) and V_3S_4 ($x = 6$) are antiferromagnetic metals with Néel temperatures of approximately 32 K and 8 K respectively, and VS ($x = 8$) is a paramagnetic metal [3–9]. The family may be expanded further with Se or Te in place of S and other transition-metal elements in place of V. Under suitable conditions the itinerant carriers in vanadium sulphides may condense into unconventional forms of superconductivity, including those anticipated to emerge on the border of magnetism [10] and charge-density-waves [11, 12]. The vanadium sulphides have also been identified as an important platform for energy technologies due to their excellent electrochemical properties and subsequent performance as electrode materials in metal-ion batteries and supercapacitors [13, 14].

V_5S_8 and V_3S_4 may be thought of as particularly stable and ordered phases of VS_2 intercalated with additional vanadium between the layers. This results in metal-full layers and metal-deficient layers as shown in figure 1(a) for V_5S_8. Antiferromagnetic V_5S_8 and V_3S_4 have been of long standing interest in the field of metallic magnetism where the degree of itinerancy of the magnetic electrons along with the importance of spin-fluctuation corrections to the thermal properties have been investigated [4–6, 9, 15–23]. In the case of V_5S_8, nuclear magnetic resonance [7] and neutron scattering [8] experiments have identified the presence of three different types of vanadium ions, V_I between the layers and V_{II} and V_{III} within the layers (see figure 1). The V_I sites alone predominantly host magnetic electrons which order below the Néel temperature, T_N, with an orthorhombic (slightly distorted face-centred-tetragonal) spin lattice as shown in figure 1(b). The low temperature atomic moment is of the order of 1.5 μ_B per V_I site so that a description in terms of a Heisenberg spin model may be appropriate to a first approximation for the bulk properties. However, as in the case of magnetic metals such as iron and cobalt with equally large moments, the Fermi surface is likely to be described by an itinerant-electron or Stoner model [15–17, 19].

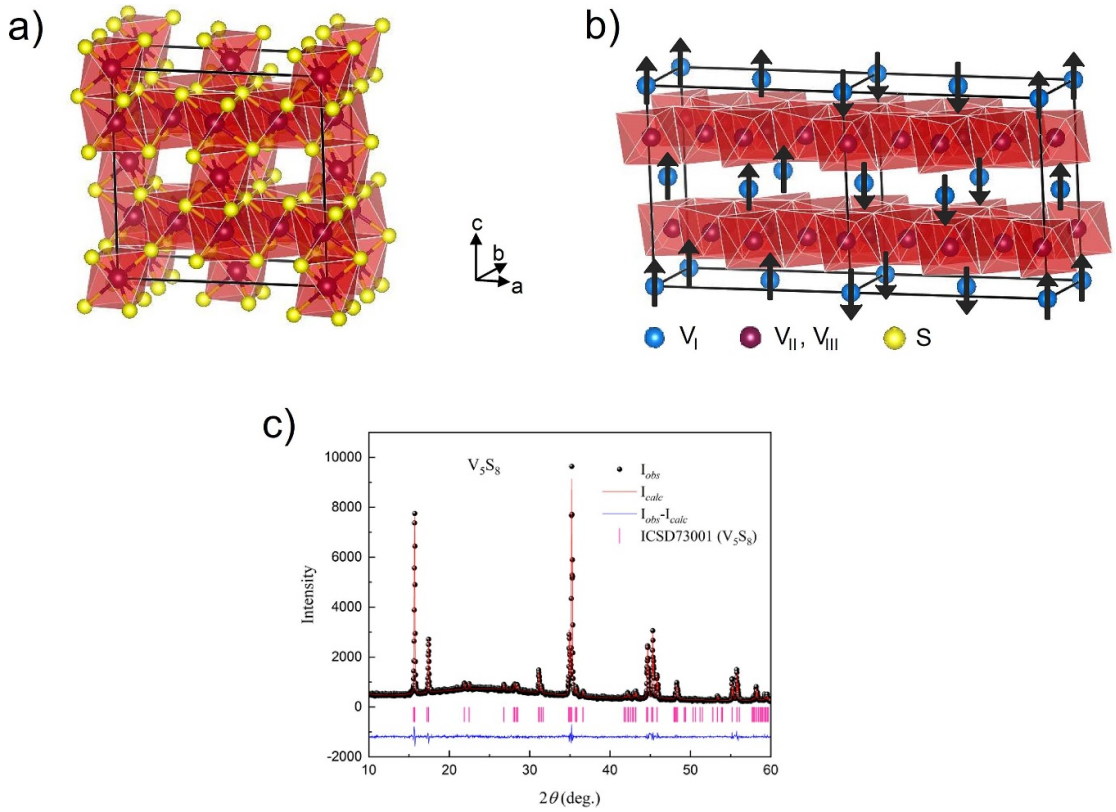

Figure 1. The crystal structure of V_5S_8 is shown in (a) in which vanadium ions are depicted as purple or blue spheres and sulphur ions as yellow spheres. The black lines indicate the unit cell of the monoclinic structure with space group F12/m1 and the orientation depicted is shown by the crystallographic axes labels *a*, *b* and *c*. The faces of polyhedra formed by sulphur ions which enclose individual vanadium ions are shaded in red. V_5S_8 is based on alternating metal-full layers involving V_{II} and V_{III} ions and metal-deficient layers involving V_I ions. The lattice parameters can be found in supplementary material. The magnetic structure of V_5S_8 below the Néel temperature [8] is shown in (b) in which the spins of magnetic electrons represented by arrows reside on the V_I sites found in the metal-deficient layers. (The sulphur ions and polyhedra surrounding V_I sites have been hidden for clarity in (b).) The results of x-ray diffraction experiments of single crystals of V_5S_8 grown for our study are presented in (c) with the powder diffractogram shown in black and Rietveld refinement phase shown in red. The positions of the observable peaks of the V_5S_8 phase are shown as magenta vertical bars. The blue line represents the difference between the observed pattern and the calculated one for a single phase material.

As a first step in the search for exotic condensates in the magnetic vanadium chalcogenides we have carried out measurements of principal thermal properties of stabilised samples of V_5S_8 at ambient pressure. The experiments summarised below reveal an unexpected and anomalous magnetic field and temperature dependence of thermodynamic quantities. Instead of the two field-induced magnetic transitions predicted by the spin-flop and spin-flip model, in V_5S_8 we observe three transitions for magnetic fields aligned along the easy axis of magnetisation, *c*, below T_N. The possible origin of this unexpected finding will be considered and discussed below after presenting the results of magnetic, electrical transport and thermal measurements.

2. Results and discussion

Multiple batches of single crystals of vanadium sulphide metals were prepared by the vapour transport technique [24–27] and were confirmed by x-ray crystallography experiments to form in a single crystallographic phase with the conventionally accepted lattice structure and stoichiometry (see figure 1(c) and Methods). The x-ray diffraction (XRD) data were obtained from powdered material made from several single crystals. The powder XRD measurements showed that the single phase samples had crystallised with lattice parameters $a = 11.38$ Å, $b = 6.65$ Å, $c = 11.31$ Å, $\alpha = 90°$, $\beta = 91.46°$, $\gamma = 90°$ and volume $= 855.24$Å^3. The parameters match the space group F 1 2 m 1 having a monoclinic structure (also referred to as C1 2 m1 in alternative nomenclature). After Rietveld refinement, it was possible to obtain an estimate of the stoichiometry of the atomic ratio of vanadium to sulphur of 5:7.95. Energy dispersive x-ray spectroscopy (EDS) was performed and gave an atomic ratio of vanadium to sulphur of 5:7.91 close to the result obtained from XRD.

The magnetic susceptibility as a function of temperature, T, and the magnetisation as a function of applied magnetic field, B_0, along the three principal crystallographic axes of single crystals were measured using a commercial superconducting quantum interference device magnetometer. The results for V_5S_8 are shown in figure 2. The susceptibility plotted against T in figure 2(a) shows moderate anisotropy above T_N and strong anisotropy below T_N where the susceptibility along the easy, c, axis falls below that along the a and b axes, as expected for an antiferromagnetically ordered state. The magnetisation versus B_0 along the c-axis plotted in figure 2(b) at a series of temperatures, shows a steep rise at a critical field of about 4.5 T in the low temperature limit ($T \ll T_N$), qualitatively as expected for spin-flop transitions which have been observed in a number of antiferromagnetic materials. Signatures of this transition are also observed in transport properties as labelled by B_1 in figures 2(d)–(f). The temperature and field dependence of the heat capacity and magnetoresistance, however, are suggestive of additional field-induced transitions.

The heat capacity of V_5S_8 as a function of T and B_0 was measured using a standard relaxational technique and the results are presented in figure 2(c). The heat capacity plotted against T in the inset of figure 2(c) shows a sharp peak which falls in amplitude and temperature as B_0 is increased. In the low field limit, the peak appears at approximately at 32 K, the accepted value of the Néel temperature. However as shown on an expanded scale in the main plot and in dC_p/dT in figure 2(e), the heat capacity peak splits apart with increasing B_0 pointing to the existence of an unexpected additional transition line. The magnetoresistance, $R(B_0)$ was measured up to 35 T using as DC resistive magnet. The new transition B_2 is clearly observed in $R(B_0)$ (figure 2(d)) and in dR/dB_0 (figure 2(f)) as being located between the spin-flop (B_1) and spin-flip (B_3) transitions. The magnetic field–temperature phase diagram shown in figure 3, which is compiled from features in the magnetisation, heat capacity and resistivity data, shows the presence of the three transition lines labelled B_1, B_2 and B_3 that decrease with increasing temperature and meet near T_N, possibly leading to two triple points or a single quadruple point. All transition lines were traced down towards absolute zero where three magnetic quantum phase transitions are revealed at $T = 0$ K with critical values $B_1 \approx 5$ T, $B_2 \approx 18$ T and $B_3 \approx 27$ T. For the measurements leading to the results shown in figure 2, at least half a dozen single-phase single-crystal specimens were selected from the different crystal-growing batches referred to above with the main findings reproducible in all crystals measured. A triad of transition lines as found here is not a widely observed characteristic of antiferromagnetic materials [28–31].

In an attempt to understand our observations in figures 2 and 3, we begin by considering a uniform antiferromagnetic chain extended along the y direction with the easy axis of magnetisation along the z direction, in a simple mean field approximation. The ground state magnetic energy of a single antiferromagnetically aligned pair at neighbouring sites i and $i-1$ in the presence of single-ion anisotropy and an applied magnetic field B_0 directed along the z axis is taken to be of the form)

$$\frac{E_{\text{pair}}}{g\mu_B\langle S\rangle} = -B_{\text{exc}}\cos(\theta_i - \theta_{i-1}) - \frac{1}{2}B_{\text{an}}\left(\cos^2\theta_i + \cos^2\theta_{i-1}\right) - B_0(\cos\theta_i + \cos\theta_{i-1}) \tag{1}$$

where $\langle S\rangle$ is the magnitude of the average spin on each site, $B_{\text{exc}} = -\frac{J\langle S\rangle}{g\mu_B}$ is an exchange field that anti-aligns the two moments when the exchange coupling $J > 0$, and B_{an} is the local uniaxial anisotropy field tending to align the spins along the z axis [32–34]. The variable θ_i is the angle between the z axis and a spin at site i which can rotate in the z–y plane to minimise the total energy. The total ground state magnetic energy for the lattice, E_{lattice}, in the mean field approximation is given by E_{pair} times the number of pairs but with the exchange term doubled to take account of the exchange contribution from the bonds between the pairs.

The spin pairs are anti-aligned for $B_0 = B_{\text{exc}}$, and aligned in the opposite limit but the transition is not continuous. Minimising E_{lattice} shows that for a range of parameters there exits a first order 'spin-flop' transition to partial spin polarisation at a value of B_0 that scales as $\sqrt{B_{\text{an}}B_{\text{exc}}}$ followed by a second order 'spin-flip' transition to full spin polarisation at B_0 that scales as B_{exc} (figure 4(a)). At the spin-flop transition the spin angles for a pair suddenly jump from $\theta_i = 0$, $\theta_{i-1} = -\pi$ to $\theta_i = -\theta_{i-1} = \theta = \theta_{\text{SF}}$, where $0 < \theta_{\text{SF}} < \frac{\pi}{2}$. The angle θ continuously decreases with increasing B_0 from θ_{SF} but does not smoothly tend to zero at infinity; instead θ vanishes at a finite spin-flip transition field. At the spin-flop field, the applied field overcomes the tendency of the exchange field together with the anisotropy field to align the spins in a pair in opposite directions along the z axis.

In the above model there are only two transitions. However further transitions can arise in more general forms of the pair energy. In particular, the inclusion of anisotropy in the two-spin and single-spin terms can lead to three transitions, qualitatively as observed in V_5S_8. To see this we generalise E_{pair} to the form)

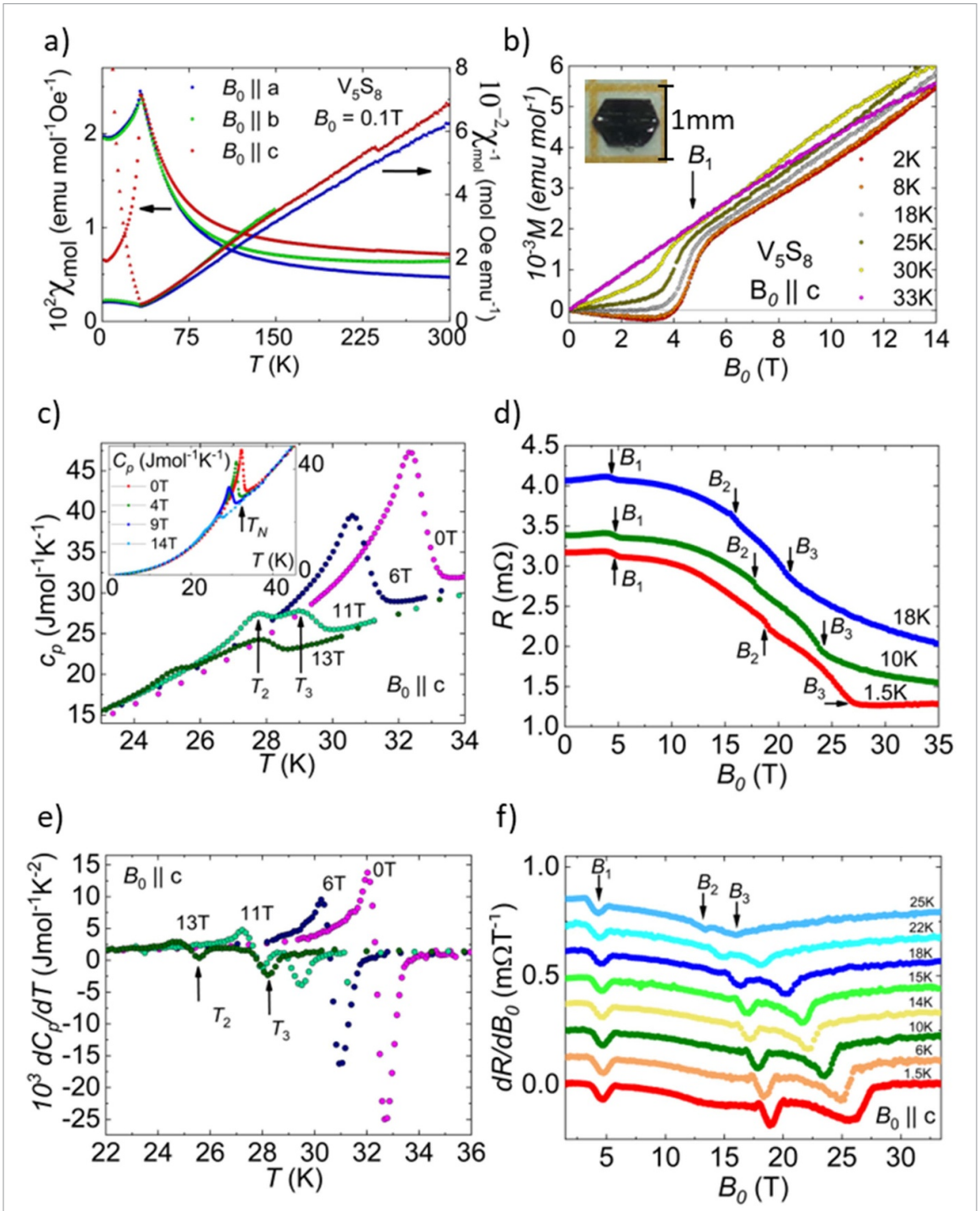

Figure 2. Magnetic, thermal and electrical measurements in V_5S_8. In (a) the magnetic susceptibility, χ_{mol}, of V_5S_8 versus temperature is plotted for the three principal crystallographic directions at a low applied magnetic field. In (b) the magnetisation, M, of V_5S_8 is plotted against applied magnetic field aligned along the easy, c, axis at a series of temperatures up to just above $T_N \approx 32$ K. The spin-flop transition field, B_1, is visible as a step in the magnetisation below T_N. The inset of (b) shows a photograph of one of the representative single crystal specimens measured. In (c) the heat capacity vs. temperature is plotted at a series of applied magnetic fields, B_0, aligned along the easy, c, axis. The figure highlights the splitting of the transition in applied magnetic fields as shown by peaks in temperature labelled T_2 and T_3 (associated with B_2 and B_3). The inset is a plot of the heat capacity data over a wider range in T at a few fields between 0 T and 14 T. The Néel temperature is visible as the steepest step at zero field near 32 K (red points). In (d) the resistance is plotted against magnetic field up to 35 T for three different representative temperatures below T_N. The three field-induced transitions are labelled B_1, B_2 and B_3 and are observed as sharp drops or kinks in $R(B_0)$. The quantities in (a)–(c) are plotted per mole of V_5S_8 which has a relative molecular mass, $M_r = 511.23$ g mol^{-1} and density, $\rho = 3.95$ g cm^{-3}. The conventional cell contains four V_I ions out of a total of twenty vanadium ions, and one V_I ion per V_5S_8 molecule in the primitive cell. Figure parts (e) and (f) show the derivatives of the quantities shown in figures (c) and (d) respectively, in which the spin transitions appear with even more clarity.

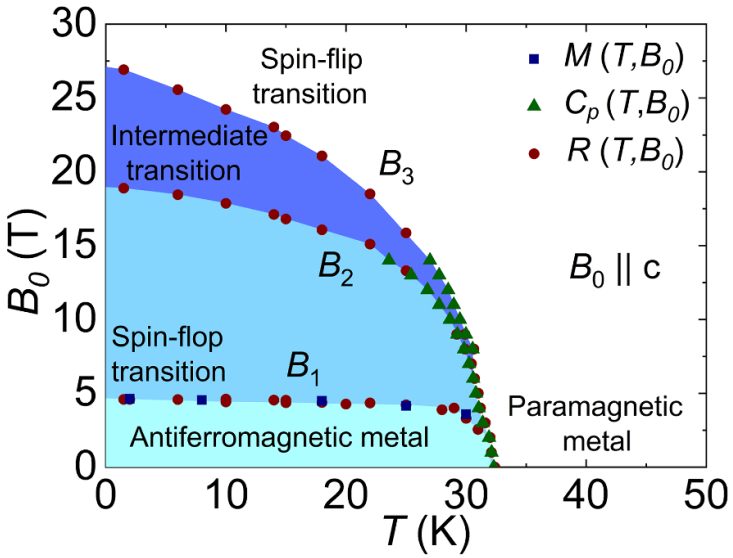

Figure 3. The triad of transition lines in V_5S_8. The applied magnetic field vs. temperature phase diagram is compiled from the data presented in figure 2 and shows the temperature dependence of the three field-induced transitions, B_1, B_2 and B_3. An unconventional intermediate spin transition is detected between the spin-flop and spin-flip transitions. The experimentally observed intermediate transition is consistent with the model outlined in the main text and presented in figure 4.

$$\frac{E_{\rm pair}}{g\mu_B\langle S\rangle} = -\left(B_z^{\rm exc}\cos\theta_i\cos\theta_{i-1} + B_y^{\rm exc}\sin\theta_i\sin\theta_{i-1}\right) - \frac{1}{2}B_z^{\rm an}\left(\cos^2\theta_i + \cos^2\theta_{i-1}\right) - \frac{1}{2}B_y^{\rm an}\left(\sin^2\theta_i + \sin^2\theta_{i-1}\right) - B_0(\cos\theta_i + \cos\theta_{i-1}) \quad (2)$$

where we have replaced $\cos(\theta_i - \theta_{i-1})$ by $\cos\theta_i\cos\theta_{i-1} + \sin\theta_i\sin\theta_{i-1}$ and included not only z but also y components of the two-site and single-site fields. Minimisation of the generalised form of $E_{\rm lattice}$ leads to two transitions if the single site anisotropy term tends to favour spin alignment along the z axis ($B_z^{\rm an} > B_y^{\rm an}$), as shown in figures 4(a) and (b). However, when the combined effects of the two-site and single-site terms make the z axis the eas$y$ axis as above, but the single site term on its own favours spin alignment along the y axis ($B_z^{\rm an} < B_y^{\rm an}$) then three phase transitions are predicted for a range of model parameters, as shown in figures 4(c) and (d). In the latter case the conflicting tendencies of terms in $E_{\rm lattice}$ for alignment along the z axis and y axis leads to a splitting of the first-order spin-flop transition into two second-order transitions B_1 and B_2. In the intermediate state between B_1 and B_2, the alignment of the two spins is given by $\theta_i = \zeta + \theta$ and $\theta_{i-1} = \zeta - \theta$, where ζ varies continuously from $\frac{\pi}{2}$ at B_1 to 0 at B_2. The second-order spin-flip transition at still higher fields where θ also vanishes is labelled B_3.

The above chain model can be generalised to the case of two sublattices for which the two site energy is replaced by an inter-sublattice coupling and the single-site energy is replaced by an intra-sublattice energy, the phenomenological parameters generalised accordingly. The qualitative form of the resulting lattice magnetic energy in the mean field approximation is similar to that given above, which under suitable conditions can lead to the same triad of magnetic transitions shown in figures 4(c) and (d) in terms of phenomenological model parameters. This proposal for the possible origin of the three magnetic transitions provides only one direction to pursue and to go further requires a more realistic model of the rather complex and unusual spin structure of V_5S_8. Intriguingly the model outlined here suggestive of three second-order phase transitions and the experimental findings shown in figure 3 implies V_5S_8 contains three field-tuned magnetic quantum phase transitions at absolute zero. These may be compared and contrasted with field-tuned magnetic quantum critical points in other system [35–40] and invites further study. Furthermore, this discussion provides some instruction for more penetrating experimental investigations in particular by means of elastic and inelastic neutron scattering measurements of the magnetic structure and spin excitations in V_5S_8 as a function of applied magnetic field with polarised neutrons. It is notable that the magnetoresistance in figure 2(d) has a similar form to the field dependence of the angle θ in figure 4(d), suggestive of the origin of electron scattering in a magnetic field in V_5S_8 and providing further experimental evidence for the model result shown in figure 4(d). A similar triad of transitions might be observable in other members of the material family such as V_5Se_8, but perhaps less probable in the V_3S_4 and V_3Se_4 variants which host a much weaker and likely more itinerant form of magnetism.

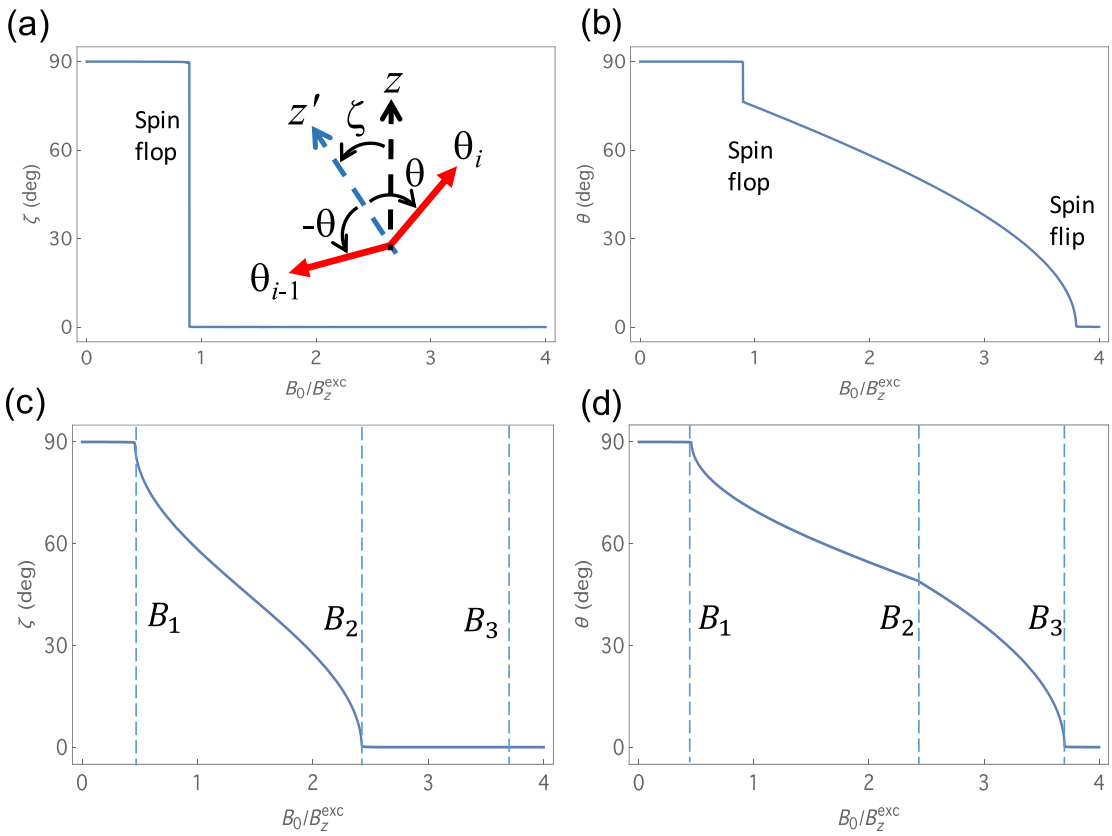

Figure 4. Magnetic field-induced transitions in the mean field approximation for the lattice spin model described in the main text including anisotropic inter-sublattice and intra-sublattice energies and the Zeeman energy. Plots (a) and (c) show ζ versus field and (b) and (d) show θ versus field. For illustration the model parameters have been chosen to be $B_y^{exc}/B_z^{exc} = 1.0$ and $(B_z^{an} - B_y^{an})/B_z^{exc} = 0.2$ in (a) and (b), and $B_y^{exc}/B_z^{exc} = 0.1$ and $(B_z^{an} - B_y^{an})/B_z^{exc} = -1.5$ in (c) and (d), and the results shown in the figures were obtained by numerical minimisation of the magnetic lattice energy $E_{lattice}$ for the ground state as outlined in the main text. The inset in (a) indicates the definitions of the angles θ and ζ. θ_i is the angle of a spin at site i as measured from the z' direction. ζ is the angle of the z' direction as measured from the z axis. The orientations of the spins represented by red arrows are able to vary in the z -y plane in order to minimise the energy. In the latter set of parameters in (c) and (d), the intra-sublattice coupling favours spin alignment along the y axis and the first-order spin-flop transition splits into two second-order transitions leading to three field-induced second-order transitions B_1, B_2 and B_3 similar to those observed in V_5S_8 (figures 2 and 3).

3. Conclusions

We report on the striking observation of a triad of magnetic phase transitions in V_5S_8 revealed by experiments in magnetic fields up to 35 T below the Néel temperature. The field-induced transitions point to the possible splitting of the spin-flop transition into two transitions, forming phases in which the alignment of the sublattice spins take on an unconventional form. The transitions terminate at three distinct magnetic quantum phase transitions at absolute zero. The results may be relevant to numerous other antiferromagnetic metals with related crystal structures and to the study of field-induced magnetic quantum phase transitions in general.

4. Methods

Single crystal specimens of V_5S_8 were grown by chemical vapour transport [27]. In a typical procedure the reagents were prepared by mixing vanadium pieces with a purity of 99.99% and sulphur powder with a purity of 99.999% in the mass ratio appropriate for the desired stoichiometry. Vanadium pieces were pre-cleaned via acid etching and heating to high temperature in vacuum followed by a final acid-etching and cleaning step. Quartz growth ampoules were also pre-cleaned via acid etching followed by heating in vacuum to 1000 °C for 24 h to degas any impurities trapped inside the walls. The ampoules were etched again in a saturated solution of KOH in isopropyl alcohol followed by flame polishing the quartz. The reagents were then sealed together inside one end of an evacuated quartz ampoule, with an argon partial pressure, and iodine (purity 99.999%) as a transport agent at an amount of 20 mg per cubic cm of the ampoule volume. The entire length of the sealed ampoule was heated to 675 °C in a two-zone tubular furnace for a few hours. The unoccupied end of the ampoule, the growth end, was

then cooled to 600 °C to form a temperature gradient. Single-crystal growth was allowed to continue at the cold end for 15 d followed by slow cooling to room temperature over 2.5 d. Samples obtained were shiny hexagonal-shaped single-crystal platelets (see inset of figure 2(b)) of typical dimensions 1 mm x 1 mm x 0.2 mm with the surfaces cleaned by etching in HCl before measurements of magnetic, electrical and thermal properties. The crystals were characterised by XRD and energy-dispersive EDS to confirm the crystal structure and stoichiometry. Susceptibility and magnetisation measurements were performed using a commercial superconducting quantum interference device (SQUID) magnetometer with a set-up to ensure alignment of the sample with the applied magnetic field. Heat capacity measurements were carried out using a standard relaxational technique down to 0.5 K and in fields up to 14 T. Resistivity measurements were performed using a standard four-contact method at temperatures down to 0.5 K and fields up 35 T. The resistivity data at high fields were collected using a DC resistive electromagnet at the National High Magnetic Field Laboratory in Tallahassee, Florida, U.S.A.

Data availability statement

All data that support the findings of this study are included within the article (and any supplementary files).

Acknowledgment

We would like to thank R. J. Cava for helpful discussions. Financial support was provided by the Royal Society, the Henry Royce Institute under EPSRC Grant Numbers EP/R00661X/1, an EPSRC Doctoral Prize award (P.M.T.V.) and a FAPESP grant with award number 2017/10581-1. A portion of this work was performed at the National High Magnetic Field Laboratory, Tallahasse, Florida, USA, which is supported by a National Science Foundation Cooperative Agreement with reference number DMR-2128556, and the State of Florida.

Author contributions

C A Sonego 0000-0002-0104-3411
Conceptualization (equal), Data curation (lead), Formal analysis (equal), Investigation (lead), Methodology (lead), Project administration (equal), Writing – original draft (equal), Writing – review & editing (equal)

P M T Vianez
Data curation (equal), Investigation (equal), Methodology (equal), Writing – review & editing (equal)

H Li
Data curation (supporting), Methodology (supporting), Writing – review & editing (equal)

J C Lashley
Investigation (equal), Methodology (equal), Writing – review & editing (equal)

G G Lonzarich
Data curation (equal), Formal analysis (equal), Methodology (equal), Writing – original draft (equal), Writing – review & editing (equal)

M N Ali
Conceptualization (supporting), Investigation (equal), Methodology (equal), Visualization (equal), Writing – review & editing (equal)

M A Avila 0000-0002-3796-3244
Funding acquisition (equal), Investigation (equal), Methodology (equal), Project administration (equal), Resources (equal), Supervision (equal), Writing – review & editing (equal)

S E Rowley 0000-0001-5350-2459
Conceptualization (lead), Data curation (equal), Formal analysis (equal), Funding acquisition (lead), Investigation (equal), Methodology (equal), Project administration (lead), Resources (equal), Supervision (lead), Validation (equal), Visualization (equal), Writing – original draft (lead), Writing – review & editing (equal)

References

[1] van Efferen C *et al* 2021 A full gap above the Fermi level: the charge density wave of monolayer VS_2 *Nat. Commun.* **12** 6837
[2] Mulazzi M *et al* 2010 Absence of nesting in the charge-density-wave system 1 T-VS_2 as seen by photoelectron spectroscopy *Phys. Rev. B* **82** 1–6
[3] Kawada I, Nakano-Onoda M, Ishii M, Saeki M and Nakahira M 1975 Crystal structures of V_3S_4 and V_5S_8 *J. Solid State Chem.* **15** 246–52
[4] Oka Y, Kosuge K and Kachi S 1974 Magnetic properties of V_5S_8 *Phys. Lett. A* **50** 311–2
[5] Nozaki H, Umehara M, Ishizawa Y, Saeki M, Mizoguchi T and Nakahira M 1978 Magnetic properties of V_5S_8 single crystals *J. Phys. Chem. Solids* **39** 851–8
[6] Kitaoka Y, Yasuoka H, Oka Y, Kosuge K and Kachi S 1979 Observation of the antiferromagnetic order in metallic compounds V_3S_4 and V_3Se_4 *J. Phys. Soc. Jpn.* **46** 1381–2
[7] Kitaoka Y and Yasuoka H 1980 NMR investigations on the spin fluctuations in itinerant antiferromagnets. II. V_3S_4 and V_5S_8 *J. Phys. Soc. Jpn.* **48** 1949–56
[8] Funahashi S, Nozaki H and Kawada I 1981 Magnetic structure of V_5S_8 *J. Phys. Chem. Solids* **42** 1009–13
[9] Fujimori A, Saeki M and Nozaki H 1991 Electron correlation, d-band formation, and magnetism in V_5S_8: photoemission-spectroscopy study *Phys. Rev. B* **44** 163–9
[10] Monthoux P, Pines D and Lonzarich G G 2007 Superconductivity without phonons *Nature* **450** 1177
[11] Kusmartseva A F, Sipos B, Berger H, Forró L and Tutiš E 2009 Pressure induced superconductivity in pristine 1T-$TiSe_2$ *Phys. Rev. Lett.* **103** 2–5
[12] Sahoo S, Dutta U, Harnagea L, Sood A K and Karmakar S 2020 Pressure-induced suppression of charge density wave and emergence of superconductivity in 1 T− VSe 2 *Phys. Rev. B* **101** 14514
[13] Wang W, Sun Z, Zhang W, Fan Q, Sun Q, Cui X and Xiang B 2016 First-principles investigations of vanadium disulfide for lithium and sodium ion battery applications *RSC Adv.* **6** 54874–9
[14] Zhang C Y, Sun G W, Liu Q Y, Pan J L, Wang Y C, Zhao H, Sun G Z, Gao X P, Pan X J and Zhou J Y 2021 Deciphering the catalysis essence of vanadium self-intercalated two-dimensional vanadium sulfides (V_5S_8) on lithium polysulfide towards high-rate and ultra-stable Li-S batteries *Energy Storage Mater.* **43** 471–81
[15] Lonzarich G G 1997 The magnetic electron GG LONZARICH *Electron: A Centenary Volume* ch 6, p 109
[16] Moriya T 2012 *Spin Fluctuations in Itinerant Electron Magnetism* vol 56 (Springer)
[17] Kulikov N I and Tugushev V V 1984 Spin-density waves and itinerant antiferromagnetism in metals *Sov. Phys. - Usp.* **27** 954
[18] Tazuke Y, Satō T and Miyako Y 1982 Susceptibility and specific heat studies on V_3S_4 *J. Phys. Soc. Jpn.* **51** 2131–5
[19] Knecht M, Ebert H and Bensch W 1998 Electronic and magnetic properties of V_5S_8 *J. Phys. Condens. Matter* **10** 9455
[20] Nakanishi M, Yoshimura K, Kosuge K, Goto T, Fujii T and Takada J 2000 Anomalous field-induced magnetic transitions in V_5X_8 (X = S,Se) *J. Magn. Magn. Mater.* **221** 301–6
[21] Hardy W J, Yuan J, Guo H, Zhou P, Lou J and Natelson D 2016 Thickness-dependent and magnetic-field-driven suppression of antiferromagnetic order in thin V_5S_8 single crystals *ACS Nano* **10** 5941–6
[22] Lonzarich G G and Taillefer L 1985 Effect of spin fluctuations on the magnetic equation of state of ferromagnetic or nearly ferromagnetic metals *J. Phys. C* **18** 4339
[23] Lonzarich G G 1986 The magnetic equation of state and heat capacity in weak itinerant ferromagnets *J. Magn. Magn. Mater.* **54** 612–6
[24] Saeki M, Nakano M and Nakahira M 1974 Crystal growth of nonstoichiometric V_5S_8 by chemical transport *J. Cryst. Growth* **24–25** 154–7
[25] Taniguchi M, Wakihara M and Shirai Y 1980 Growth of single crystals of vanadium sulfides and their electrical conductivity *ZAAC—J. Inorg. Gen. Chem* **461** 234–40
[26] Wakihara M, Kinoshita K, Hinode H and Taniguchi M 1982 Growth of single crystals of vanadium sulfides and some thermodynamic considerations for the vapor transport process *J. Cryst. Growth* **56** 157–62
[27] Sonego C A, Li H, Einarsson Nielsen P, Lashley J C, Avila M A and Rowley S E 2024 The growth of V_5S_8 single crystals by chemical vapour transport *Braz. J. Phys.* **54** 187
[28] Maruthi R, Seehra M S, Ghosh S, Medwal R, Rawat R S, Weise B, Choi E S and Thota S 2022 Determination of the tricritical point, H–T phase diagram and exchange interactions in the antiferromagnet $MnTa_2O_6$ *J. Phys. Condens. Matter* **34** 155801
[29] Maruthi R, Ghosh S, Seehra M S, Joshi D C, Chowdhury M R, Medwal R, Rawat R S, Weise B and Thota S 2021 Magnetic field-temperature phase diagram, exchange constants and specific heat exponents of the antiferromagnet $MnNb_2O_6$ *J. Phys. Condens. Matter* **33** 345801
[30] Thota S, Ghosh S, Maruthi R, Joshi D C, Medwal R, Rawat R S and Seehra M S 2021 Magnetic ground state and exchange interactions in the Ising chain ferromagnet Co Nb 2 O 6 *Phys. Rev. B* **103** 64415
[31] Maruthi R, Singh S, Ghosh S, Seehra M S, Weise B, Prellier W and Thota S 2023 Magnetic structure and field-induced transitions in the triangular spin-1 antiferromagnet $NiNb_2O_6$: observation of a triple point *Phys. Rev. B* **108** 224430
[32] Blundell S 2001 *Magnetism in Condensed Matter* (available at: https://academic.oup.com/book/54773?login=false)
[33] Van Wier O P, van Peski-tinbergen T and Gorter C J 1959 New solutions of the molecular field equations for antiferromagnetism in an orthorhombic crystal at zero temperature *Physica* **25** 116–32
[34] Yamashita N 1972 Field induced phase transitions in uniaxial antiferromagnets *J. Phys. Soc. Jpn.* **32** 610–5
[35] Sachdev S 2011 *Quantum Phase Transitions* (Cambridge University Press)
[36] Coldea R, Tennant D A, Wheeler E M, Wawrzynska E, Prabhakaran D, Telling M, Habicht K, Smeibidl P and Kiefer K 2010 Quantum criticality in an ising chain: experimental evidence for emergent e8 symmetry *Science* **327** 177–80
[37] Liang T, Koohpayeh S M, Krizan J W, McQueen T M, Cava R J and Ong N P 2015 Heat capacity peak at the quantum critical point of the transverse Ising magnet $CoNb_2O_6$ *Nat. Commun.* **6** 7611
[38] Kinross A W, Fu M, Munsie T J, Dabkowska H A, Luke G M, Sachdev S and Imai T 2014 Evolution of quantum fluctuations near the quantum critical point of the transverse field ising chain system $CoNb_2O_6$ *Phys. Rev. X* **4** 31008
[39] Grigera S A, Perry R S, Schofield A J, Chiao M, Julian S R, Lonzarich G G, Ikeda S I, Maeno Y, Millis A J and Mackenzie A P 2001 Magnetic field-tuned quantum criticality in the metallic Ruthenate $Sr_3Ru_2O_7$ *Science* **294** 329–32
[40] Kraemer C *et al* 2012 Quantum Criticality in $LiErF_4$ *Science* **1** 1416–20